J Neurooncol (2010) 99:165–176
DOI 10.1007/s11060-010-0115-y

LABORATORY INVESTIGATION - HUMAN/ANIMAL TISSUE

A novel pre-clinical in vivo mouse model for malignant brain tumor growth and invasion

Laura M. Shelton · Purna Mukherjee · Leanne C. Huysentruyt · Ivan Urits · Joshua A. Rosenberg · Thomas N. Seyfried

Received: 24 September 2009 / Accepted: 4 January 2010 / Published online: 13 January 2010
© Springer Science+Business Media, LLC. 2010

Abstract Glioblastoma multiforme (GBM) is a rapidly progressive disease of morbidity and mortality and is the most common form of primary brain cancer in adults. Lack of appropriate in vivo models has been a major roadblock to developing effective therapies for GBM. A new highly invasive in vivo GBM model is described that was derived from a spontaneous brain tumor (VM-M3) in the VM mouse strain. Highly invasive tumor cells could be identified histologically on the hemisphere contralateral to the hemisphere implanted with tumor cells or tissue. Tumor cells were highly expressive for the chemokine receptor CXCR4 and the proliferation marker Ki-67 and could be identified invading through the pia mater, the vascular system, the ventricular system, around neurons, and over white matter tracts including the corpus callosum. In addition, the brain tumor cells were labeled with the firefly luciferase gene, allowing for non-invasive detection and quantitation through bioluminescent imaging. The VM-M3 tumor has a short incubation time with mortality occurring in 100% of the animals within approximately 15 days. The VM-M3 brain tumor model therefore can be used in a pre-clinical setting for the rapid evaluation of novel anti-invasive therapies.

Keywords Glioblastoma multiforme · Invasion · Bioluminescence · CXCR4 · IGFBP-2 · Ki-67 · VM mouse

Abbreviations

CT-2A	Mouse astrocytoma
CXCR4	Chemokine receptor
GBM	Glioblastoma multiforme
IGFBP-2	Insulin-like growth factor binding protein 2
Ki-67	Proliferation marker
VM-M3	Invasive mouse malignant glioma
VM-M3/Fluc	VM-M3 tumor cells labeled with firefly luciferase
VM-NM1	Mouse malignant glioma

L. M. Shelton · P. Mukherjee · L. C. Huysentruyt · I. Urits · J. A. Rosenberg · T. N. Seyfried (✉)
Boston College, Higgins Hall 140 Commonwealth Ave., Chestnut Hill, MA 02467, USA
e-mail: seyfridt@bc.edu

Introduction

Glioblastoma multiforme (GBM) is the most common form of primary brain cancer in adults [1]. GBM has a poor outcome due to its invasive and aggressive nature. Treatments have been largely ineffective and consist of surgical resection followed by radiation and/or chemotherapy [1, 2]. Due to the invasive nature of GBM, complete surgical removal is not possible. Many GBM's are multicentric, having secondary lesions at sites distant to the primary tumor [3–5]. In addition, chemotherapy and radiation are toxic, often resulting in further brain damage [6]. Reliable models are required that focus on the invasive nature of GBM for pre-clinical studies and for drug development. Although a number of brain tumor models exist, none recapitulate all of the characteristics of a human GBM, such as the typical growth patterns and infiltrative behavior [7]. While xenograph models are attractive, the mouse hosts are immune compromised and lack an immune-mediated response as well as a syngeneic host microenvironment [8–10]. Additionally, human tumors grown as xenographs tend to lose their invasive properties when grown in vivo following in vitro culturing [11]. Tumor cell

growth patterns in xenografts also do not replicate the tumor cell growth patterns seen in humans with GBM [8, 9, 11]. New animal models for GBM are therefore needed that better reflect the properties seen in the natural host.

Chemically induced models are grown in immune competent hosts and, to date, are some of the most commonly used mouse syngeneic brain tumor models [12–15]. However, these brain tumors lack typical GBM growth patterns and extensive invasion [7, 13]. Rat brain tumor models are also available but are highly immunogenic thus complicating results of potential therapies [16]. There is also evidence of spontaneous tumor regression in some rat models of brain cancer [17]. The rat CNS-1 glioma model is useful for assessing immuno-based therapies because it is weakly immunogenic and has greater invasive properties than those seen in the more common rat glioma models to include periventricular and perivascular spread [18]. The leptomeningeal spread, however, could also be a result of the inoculation method [18]. In general, the invasive properties of most rodent models are limited to the area of the main tumor mass [9, 19]. Hence, most of the currently available rodent brain tumor models do not reflect the full spectrum of the growth and invasive characteristics of human GBM.

Due to the limitations of current brain tumor models, transgenic models have been developed based on gain of function or targeted deletions in glioma-associated genes [20]. Complicated breeding and genotyping procedures, however, are required to generate these transgenic models [20–22]. Though these transgenic models often replicate high-grade gliomas, a model with a mutation in a single pathway is not a realistic representation of the human disease because human gliomas contain a number of distinct genetic abnormalities [8, 23, 24]. Also, the tumors that develop are not always identical in morph or grade [8]. As an alternative, MMLV (moloney murine leukemia virus)-based somatic gene-transfer glioma models rely on retroviral infection of glial cells [22, 25]. This method allows for the delivery of multiple genes thus bypassing the production of additional transgenic lines [8]. However, retroviral infection is often non-specific, targeting numerous cells and resulting in heterogeneous tumors of unknown cellular origin [21, 22].

In addition to the available rodent models, a number of dog breeds are predisposed to spontaneous brain tumors to include boxers and golden retrievers [26, 27]. Some of these brain tumors are highly invasive and closely resemble the histological and growth characteristics of human GBM [9, 28]. However, dog models are not readily available and researchers would need to rely on the recruitment of recently diagnosed dogs for studies [9]. The specific grade and type of dog glioma also varies and only about 5% of all dog brain tumors are GBM [28, 29].

The inbred VM mouse strain is unique in expressing a relatively high incidence (1.5%) of spontaneous brain tumors, most of which were characterized histologically as malignant astrocytomas [30, 31]. The VM-M3 brain tumor arose spontaneously in the forebrain of a VM mouse and expresses properties of microglia/macrophages similar to that seen in several types of invasive cancers of neural origin [32–35]. The VM-M3 tumor cells are negative for the astrocyte and neuronal markers GFAP and NF200, respectively [33]. However, the VM-M3 tumor cells express high levels of the chemokine receptor gene, CXCR4, which has been linked to the invasive and malignant properties of human gliomas [19, 33, 36–38]. High CXCR4 levels are more often associated with the higher-grade gliomas, including GBM and are indicative of poor postoperative prognosis [37]. Similar to high-grade human gliomas, the VM-M3 tumor cells are highly invasive when implanted orthotopically and invading tumor cells can be found deep within the brain parenchyma [33, 39]. The VM-M3 tumor cells are weakly immunogenic and can be grown in the syngeneic VM mouse host with predictable and reproducible growth rates [33, 40]. Moreover, the invasive VM-M3 brain tumor expresses systemic metastasis when grown outside the brain [33]. While extracranial metastasis is not commonly seen in most patients with glioblastoma, it is well documented that systemic metastasis is more common for glioblastoma than for any other human brain tumor type [41–45]. Hence, the VM-M3 mouse brain tumor expresses several characteristics observed in human GBM.

In addition, the VM-M3 tumors are labeled with the firefly luciferase gene allowing for non-invasive detection of tumor growth via bioluminescent imaging [33]. Bioluminescent imaging has been developed for a number of glioma tumor model systems and is established as an accurate measurement of tumor growth over time [13, 46, 47]. Hence, the VM-M3 tumor cells manifest several characteristics seen in aggressive human malignant gliomas to include GBM. Here we describe for the first time the invasive characteristics of the VM-M3 brain tumor in the CNS using a novel bioluminescent-based invasion assay.

Methods

Mice

Mice of the VM/Dk (VM) strain were obtained as a gift from H. Fraser (University of Edinburgh, Scotland). The C57BL/6 J mice were obtained originally from the Jackson Laboratory, Bar Harbor, ME. All mice used in this study were housed and bred in the Boston College Animal Care

Facility using husbandry conditions as previously described [48]. All animal procedures were in strict accordance with the NIH Guide for the Care and Use of Laboratory Animals and were approved by the Institutional Animal Care Committee.

Tumor formation

The VM-M3 and VM-NM1 tumors used in this study arose spontaneously in the cerebrum of adult VM mice. These tumors were detected during routine examination of the VM mouse colony over a period of several years (1993–2000). Each tumor-bearing mouse expressed cranial swelling and appeared lethargic with the males also expressing priapism as we previously described [33]. These symptoms appeared for only about 1–3 days before morbidity. The tumors were grossly identified in the cerebrum as poorly defined masses (about 3 × 1 × 1 mm) similar to those described previously for other independently arising spontaneous tumors in the VM mouse brain [31, 39]. In order to preserve in vivo viability, each tumor was immediately resected and implanted intracerebrally (i.c.) into host VM mice as described below. As soon as cranial domes appeared, the tumors were passaged again into several host VM mice. After a total of three i.c. passages, the tumors were grown subcutaneously (s.c.) and cell lines were prepared from each tumor as described below. The CT-2A tumor was originally produced through implantation of 20-Methylcholanthrene into the cerebral ventricle of a B6 mouse and was broadly classified as a poorly differentiated highly malignant anaplastic astrocytoma [49].

Tumor cell preparation

Tumor cell lines were prepared as described previously [33]. Briefly, tumor tissue was removed from the mice and was transferred to a Petri dish containing Dulbecco's Modified Eagle medium (DMEM, Sigma, St. Louis, MO) with high glucose (25 mM) supplemented with 10% fetal bovine serum (FBS, Sigma) and 50 μg/ml penicillin–streptomycin (Sigma). The tumor tissue was minced thoroughly to obtain a cell suspension. 1 ml of the cell suspension was then seeded into a tissue culture flask containing DMEM (25 mM glucose, 10% FBS). The VM tumor cells were evaluated after a minimum of eight passages to insure that the cells lines were uniformly homogeneous.

Transduction of cell lines

The VM-M3 cell line was transduced with a lentivirus vector containing the firefly luciferase gene under control of the cytomegalovirus promoter (VM-M3/Fluc) as we previously described (gift from Miguel Sena-Esteves) [33].

Tumor implantation

Tumor implantation was performed as previously described [48]. Briefly mice are anaesthetized with Avertin (0.1 ml/10 g). The tops of the heads are disinfected with ethanol and a small incision is made in the scalp of the mouse over the midline. A 3 mm^3 burr hole is made in the skull over the right parietal region behind the coronal suture and lateral to the sagittal suture. Using a trocar, a small (1 mm^3) tumor fragment is implanted into the hole made in the skull. The flaps of skin are then immediately closed with collodion. Additionally, some implants were performed using approximately 10,000–20,000 cells in 5 μl PBS. The cells were injected into the right cerebral hemisphere using a Hamilton syringe. All tumor-implanted mice reached morbidity at approximately 12–15 days regardless of implant method. Both methods result in the implantation of tumor fragments or tumor cells approximately 1.5–2 mm deep into the cortical region as previously described [50]. Tumor cells are also highly invasive regardless of implant method. The mice were placed in a warm room (37°C) until they were fully recovered.

Imaging

The Xenogen IVIS system (Xenogen, Hopkington, MA) is used to record the bioluminescent signal from the labeled tumors as we recently described [33]. Briefly, for in vivo imaging, mice recieved an intraperitoneal injection of d-Lucifierin (50 mg/kg, Promega) in PBS and Avertin (0.1 ml/10 g). Imaging times ranged from 3 to 10 min, depending on the time point. For ex vivo imaging, brains were removed and sectioned down the midline. Individual hemispheres were imaged separately in 300 μg/ml d-Luciferin in PBS, and imaged from 3 to 10 min. After each hemisphere was imaged, the cerebellum, brain stem, cortex and hippocampus were removed and imaged separately in an additional 300 μg/ml d-Luciferin in PBS. The IVIS Lumina cooled CCD camera system was used for light acquisition. Data acquisition and analysis was performed with Living Image® software (Caliper LS).

RT-PCR

All cell lines were grown under identical conditions as described previously [51]. VM brain and VM-M3 tumor samples were frozen at −80°C until time of analysis. Single strand cDNA was synthesized from total RNA and used for PCR amplification as we previously described

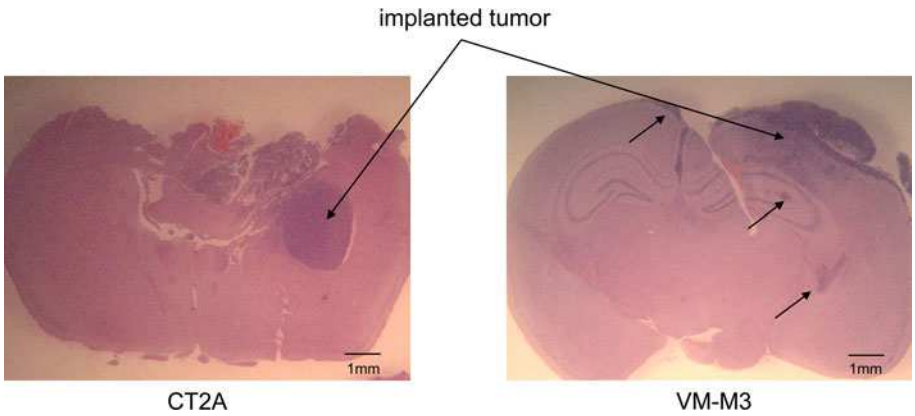

Fig. 1 Comparative analysis of the growth behavior of mouse brain tumors, VM-M3 and the CT-2A malignant astrocytoma. Small tissue fragments from the CT-2A and VM-M3 tumors were implanted into the right cerebral hemisphere (i.c.) of their syngeneic host C57BL/6J and VM strains, respectively. Brains were removed approximately 11–15 days post implantation and were stained with haematoxylin and eosin (H&E) as described in "Methods" section. The CT-2A tumor shows a distinct tumor border with little local invasion and no distant invasion. The VM-M3 tumor is highly invasive both locally and distally with numerous secondary tumor lesions (*arrows*). Images are shown at ×7.5

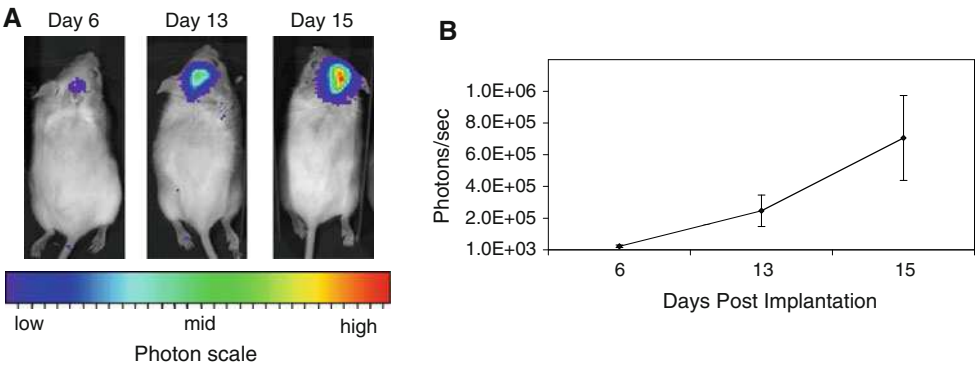

Fig. 2 Growth of the VM-M3/Fluc tumor with bioluminescence imaging. **a** VM-M3/Fluc tumor fragments were implanted as described in Fig. 1. Cranial images were taken over 15 days (representative mouse shown). **b** Bioluminescence from the whole mouse was quantified and plotted on a linear scale. All values are expressed as the mean of 6 independent samples ± SEM

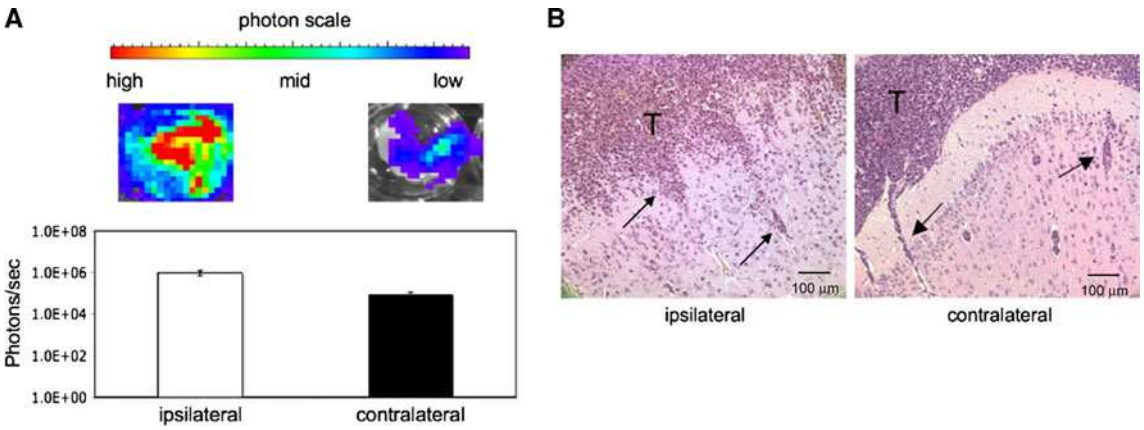

Fig. 3 Detection of VM-M3/Fluc tumor cell invasion into the contralateral hemisphere with bioluminescent imaging and histology. **a** VM-M3/Fluc tumor fragments were implanted as described in Fig. 1. Removed brains were dissected into ipsilateral and contralateral hemispheres. Each hemisphere was imaged for bioluminescence ex vivo as described in "Methods" section. Bioluminescence from each brain half was quantified and plotted on a log scale. Bioluminescence in the contralateral hemisphere is indicative of distal tumor spread. The values are expressed as means ± SEM of six independent tumor-bearing mice. **b** Histological analysis (H&E) was used to validate the presence of tumor cells in the contralateral hemisphere as described in "Methods" section. Tumor cells are shown in the contralateral hemisphere invading the neural parenchyma from the sub pial membrane (*arrows*). Images are shown at ×200

[52]. Primer sequences used for PCR were for β-actin, forward 5′-TGTGATGGTGGGAATGGGTCAG-3′ and reverse 5′-TTTGATGTCACGCACGATTTCC-3′; for IGFBP-2, forward 5′-GGGTACCTGTGAAAAGAGACG-3′ and reverse 5′-TGCAGGGAGTAGAGATGTTCC-3′; for CXCR4, forward 5′-CTACAGCAGCGTTCTCATCC-3′ and reverse 5′-GGATGACTGTCGTCTTGAGG-3′. Primers were optimized for annealing temperatures and cycle numbers as previously described [52]. RT-PCR products were separated on a 1–1.6% agarose gel containing ethidium bromide and visualized by UV light. RT-PCR was performed on the total RNA of each sample in the absence of reverse transcriptase to control for possible DNA contamination.

Confocal microscopy

Cells in culture were maintained as previously described [51]. Cells were seeded in glass-chambered slides in complete DMEM (Sigma) media. After 24 h cells were stimulated with 100 ng/ml of CXCL-12 (SDF-1) in serum free media for 30 min. Cells were washed and fixed with 4% formaldehyde for 20 min at 37°C. After blocking with 10% goat serum in 0.1% BSA, cells were incubated with CXCR4 primary antibody (1:100) for 1 h followed by secondary antibody (1:100) incubation for 1 h at room temperature. Cells were washed and stained with Hoechst for 10 min and mounted. Corresponding wells without primary antibody served as negative controls.

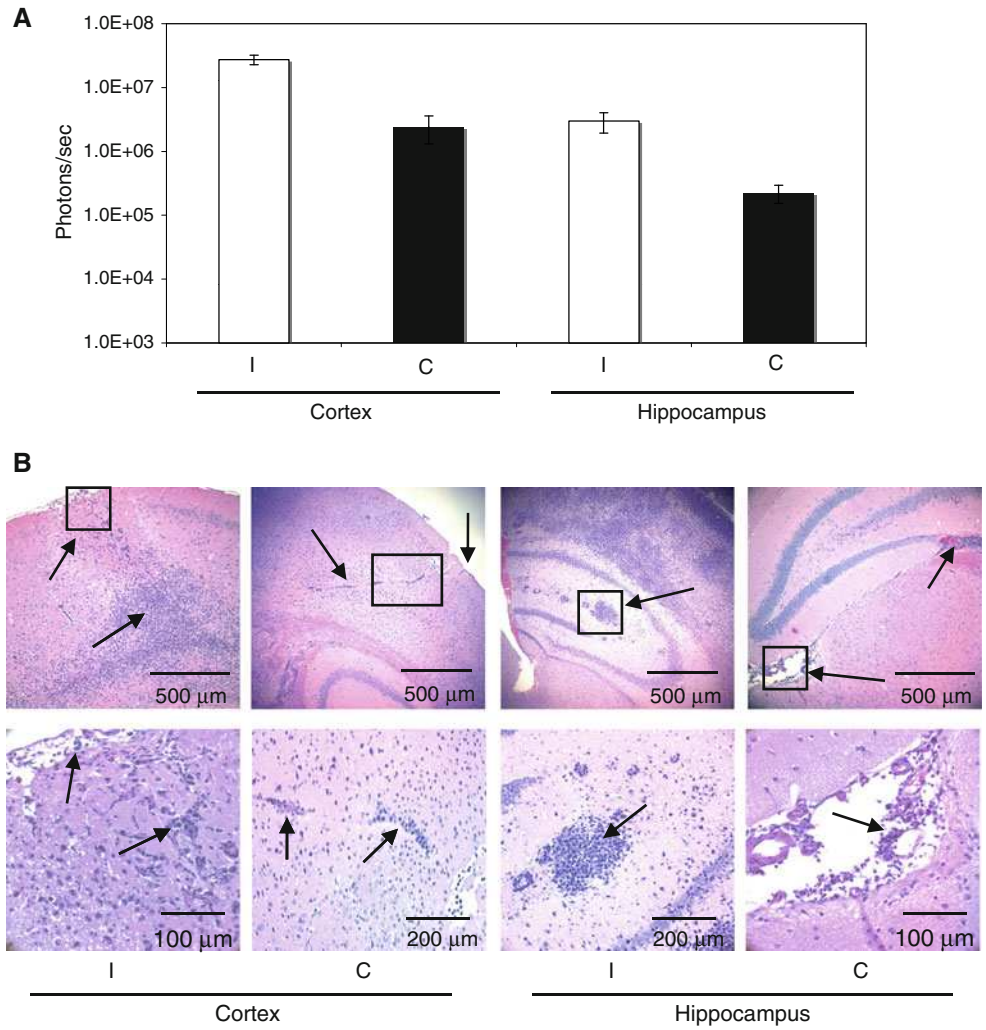

Fig. 4 Bioluminescent and histological analysis of distal tumor spread to the cortex and hippocampus. VM-M3/Fluc tumor fragments or cells were implanted as described in Fig. 1. Removed brains were sectioned through the midline and were further dissected into the cortex and hippocampus. **a** Bioluminescence was quantified and plotted on a log scale. All values are expressed as the mean ± SEM of 10 independent samples. **b** Histological analysis (H&E) was used to validate the presence of tumor cells as described in "Methods" section. *Top panel* images are shown from left to right at ×100, ×50, ×50, and ×100. The *black boxes* from the *top panel* images are shown in higher power in the *bottom panel*. *Bottom panel* images are shown from left to right at ×400, ×200, ×200, and ×400. *Arrows* indicate invasive tumor cells. I, ipsilateral; C, contralateral

For the immunohistochemical studies, the tissue sections from untreated tumor bearing mice were deparaffinized, rehydrated and washed. The tissue sections were then heat treated (95°C) in antigen unmasking solution (Vector Laboratories, Burlingame, CA) for 30 min. Tissue sections were blocked in goat serum (1:10 in PBS) for 1 h at room temperature, treated with CXCR4 primary antibody (rabbit polyclonal, 1:200 SantaCruz) in blocking buffer for 1 h at room temperature, followed by alexafluor 585 conjugated anti-rabbit secondary (Invitrogen) at 1:200 dilution for 45 min. Sections were incubated with Hoechst (10 μg/ml) for 10 min and mounted. Corresponding tissue sections without primary antibody served as negative controls. For confocal microscopy, digital images were obtained on a Leica DMI6000 inverted scope equipped with the Leica TCSSP5 confocal system, using HCX PL APO 40×/1.25 NA oil and HCX PL APO 63×/1.4 NA oil objective lenses. Leica confocal software was used to acquire images.

For Ki-67 staining, tissue slides were processed similarly as for CXCR4 and then treated with Ki-67 primary antibody (rat monoclonal, Dako, 1:100) overnight at 4°C followed by a biotinylated anti-rat secondary antibody at 1:100 dilution (Vector laboratories, Inc). The sections were then treated with avidin biotin complex followed by 3,3′-diaminobenzidine as substrate for staining according to the manufacturer's protocol (Vectastain Elite ABC kit, Vector laboratories, Inc.). The sections were counter stained with haematoxylin and mounted. Corresponding tissue sections without primary antibody served as negative controls. Bright field images were captured by a Zeiss Axioplan 2 light microscope.

Histology

Brain tumor samples were fixed in 10% neutral buffered formalin (Sigma) and embedded in paraffin. The brain-tumor samples were sectioned at 5 μm, were stained with

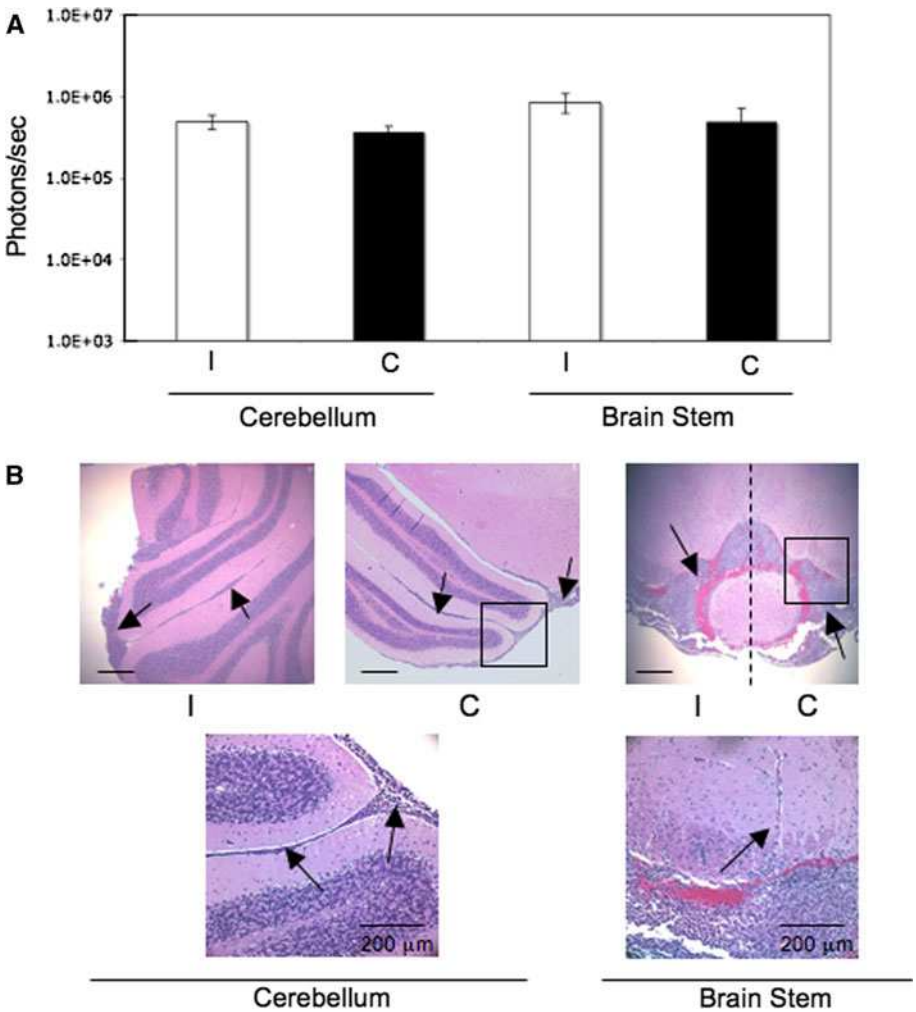

Fig. 5 Bioluminescent and histological analysis of distal tumor spread to the brain stem and cerebellum. VM-M3/Fluc tumor fragments or cells were implanted as described in Fig, 1. Removed brains were sectioned down the midline and were further dissected into cerebellum and brain stem. **a** Bioluminescence was quantified and plotted on a log scale. All values are expressed as the mean ± SEM of 10 independent samples. **b** Histological analysis (H&E) was used to validate the presence of tumor cells as described in "Methods" section. *Top panel* images are shown at ×50. The *scale bar* represents 250 μm. The *black boxes* from the *top panel* images are shown in higher power in the *bottom panel*. *Bottom panel* images are shown at ×200. *Arrows* identify subpial tumor cell spread in the cerebellum and tumor cell invasion in the brain stem. The *dashed line* demarcates the ipsilateral from the contralateral side of brain stem

haematoxylin and eosin (H&E) at the Harvard University Rodent Histopathology Core Facility (Boston, MA), and were examined by light microscopy using either a Zeiss Axioplan 2 or Nikon SMZ1500 light microscope as we previously described [14]. Images were acquired using SPOT Imaging Solutions (Diagnostic Instruments, Inc) cameras and software. All histological sections were evaluated by a veterinary neuropathologist, (Roderick Bronson) at the Harvard University Rodent Histopathology Core Facility.

Results

The objective of this study was to evaluate the potential usefulness of the VM-M3 murine brain tumor as a model for human GBM based on growth and infiltrative patterns in the CNS.

Comparison of invasive versus non-invasive brain tumors

Figure 1 shows the gross histological phenotype of the non-invasive C57BL/6 CT-2A astrocytoma model and the VM-M3 brain tumor model. The CT-2A tumor showed a sharp border with minimal local invasion and no distant invasion consistent with its previously reported behavior [12]. In contrast, the VM-M3 tumor showed a diffuse border with several secondary focal lesions within the brain parenchyma as well as in the contralateral hemisphere.

Quantitative assessment of tumor growth

We used the luciferase labeled VM-M3 tumor and monitored tumor growth non-invasively over time (Fig. 2). The bioluminescent signal could be evaluated both qualitatively (Fig. 2a), and quantitatively (Fig. 2b) during tumor progression. Bioluminescence, above the lower limit of the imaging system ($\sim 1 \times 10^3$ photons/s), could be detected as early as day 6.

Detection and quantitation of VM-M3 invading tumor cells

In order to quantitate the level of tumor invasion, the brains were removed at the end of the study and imaged ex vivo as described in "Methods" section. The brains were sectioned down the midline and each half was imaged separately. As shown in Fig. 3a, bioluminescence was detected in both the ipsilateral and the contralateral hemispheres. The level of invasion into the contralateral hemisphere was also measured. In addition, histology was used to confirm the presence of invading tumor cells in both the ipsilateral and contralateral hemispheres (Fig. 3b).

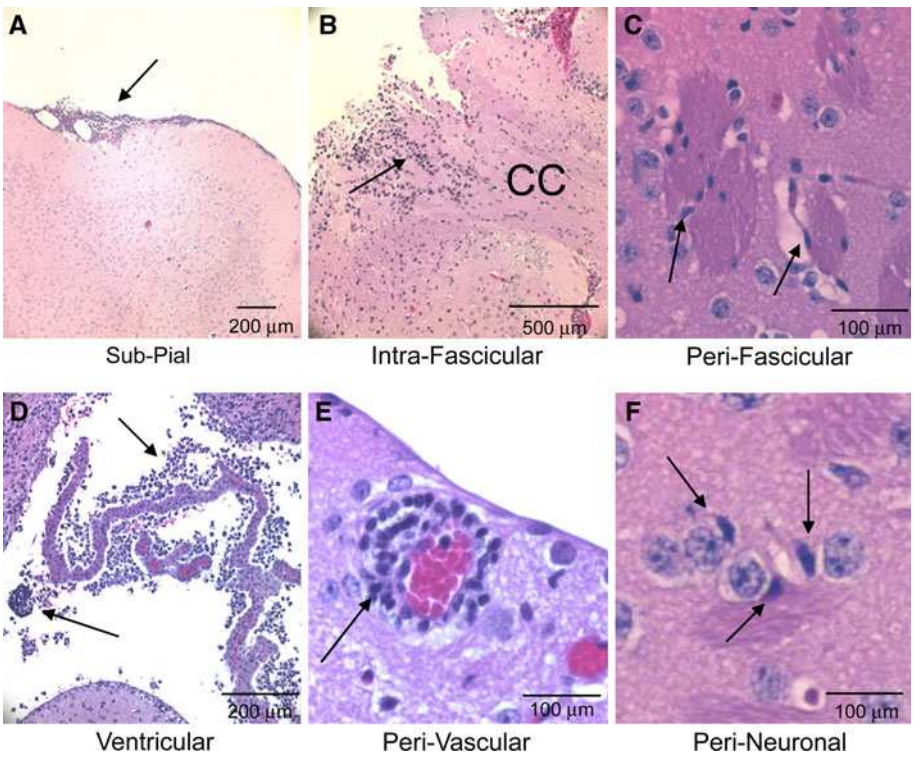

Fig. 6 Migratory routes of the VM-M3/Fluc brain tumor cells. VM-M3/Fluc tumor fragments or cells were implanted as described in Fig. 1. Histological analysis (H&E) was used to validate the presence of tumor cells as described in "Methods" section. The VM-M3/Fluc tumor cells are shown invading along the pial surface (*arrow*, **a**), within the corpus callosum (CC, *arrow*, **b**), along myelinated axons crossing through the striatum (*arrow*, **c**), through the ventricular system (*arrows*, **d**), around the blood vessels (*arrow*, **e**), and around neurons (*arrow*, **f**). Images are shown at ×100 (**a**), ×50 (**b**), ×400X (**c**), ×200 (**d**), and ×400 (**e**, **f**). *Arrows* identify regions containing tumor cells

Quantitation of distal tumor spread

In order to further evaluate the invasion of the VM-M3 tumor cells, the removed brains were dissected into the cortex, hippocampus (Fig. 4a), brain stem, and cerebellum (Fig. 5a). Using the Xenogen Imaging System, bioluminescence was detected and quantitated in all of the brain regions. Histology was used to confirm the presence of invading tumor cells in the corresponding regions (Figs. 4b, 5b).

Migratory routes of invading tumor cells

We next identified the routes of VM-M3 tumor cell invasion (Fig. 6). We identified surface or sub-pial spread as the major route of invasion (Fig. 6a). However, we also identified tumor cells invading along and within white matter tracts, such as the corpus callosum and along myelinated axons crossing through the striatum (Fig. 6b, c), through the ventricular space (Fig. 6d), along blood vessels (Fig. 6e) and along neurons (Fig. 6f).

Expression of CXCR4 and IGFBP-2 in brain, tumor tissue, and cultured tumor cells

As shown in Fig. 7a, the VM-M3 tumor cells both in vivo and in vitro expressed high levels of CXCR4, a chemokine receptor highly expressed in human GBM. In addition, the less invasive VM-NM1 tumor from the same VM mouse host had very low CXCR4 gene expression. Also, we showed that insulin-like growth factor binding protein 2 (IGFBP-2) was not highly expressed in the invasive VM-M3 cells whereas the less invasive VM-NM1 tumor cells had high expression of IGFBP-2. We also found that CXCR4 was localized to the perimeter of the VM-M3 tumor cells that were grown either in vivo or in vitro (Fig. 7b). Additionally, CXCR4 expression was found in the cells that had invaded throughout the brain via the sub-pial space, white matter tracts, and blood vessels (Fig. 8).

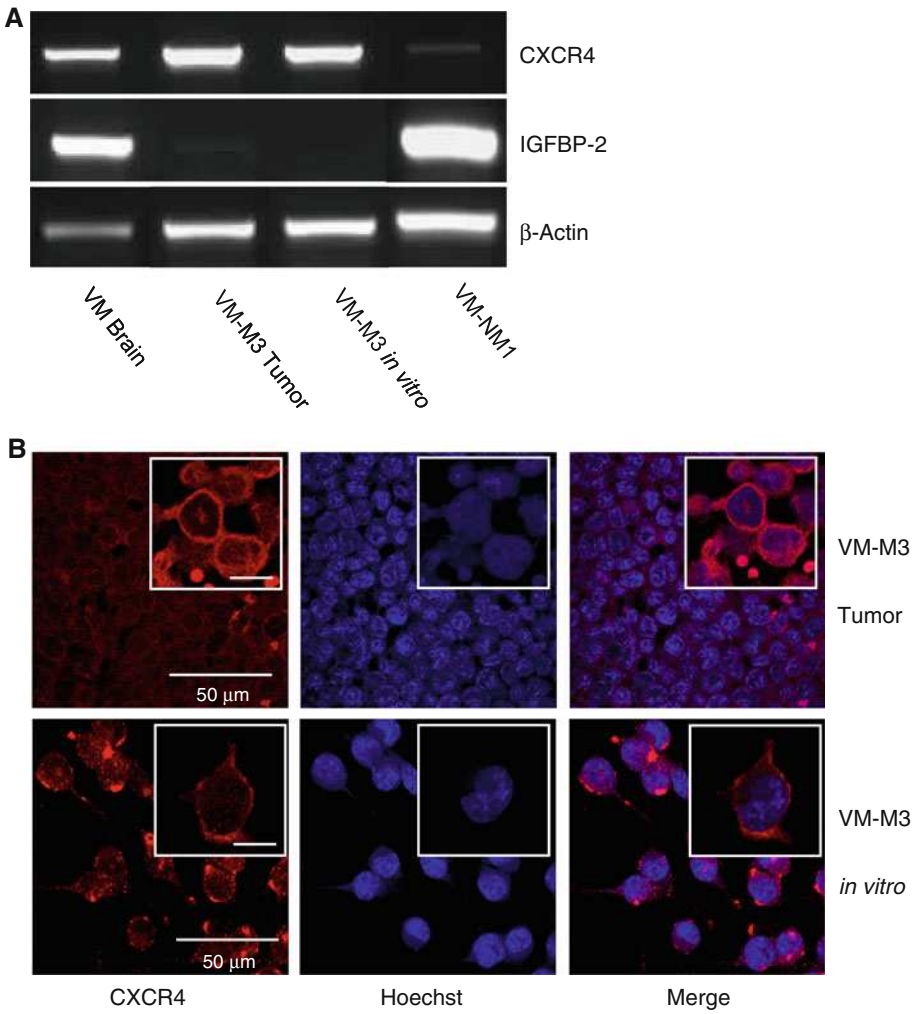

Fig. 7 Expression of CXCR4 and IGFBP-2 in brain, tumor tissue, and in cultured tumor cells. **a** CXCR4 and IGFBP-2 gene expression was determined by semi-quantitative RT-PCR as described in "Methods" section. **b** CXCR4 protein localization was determined in vitro following SDF-1 stimulation and in vivo as described in "Methods" section. Images are shown at ×400 and ×630 (*insert*). *Scale bars* in the *insert* represent 10 μm

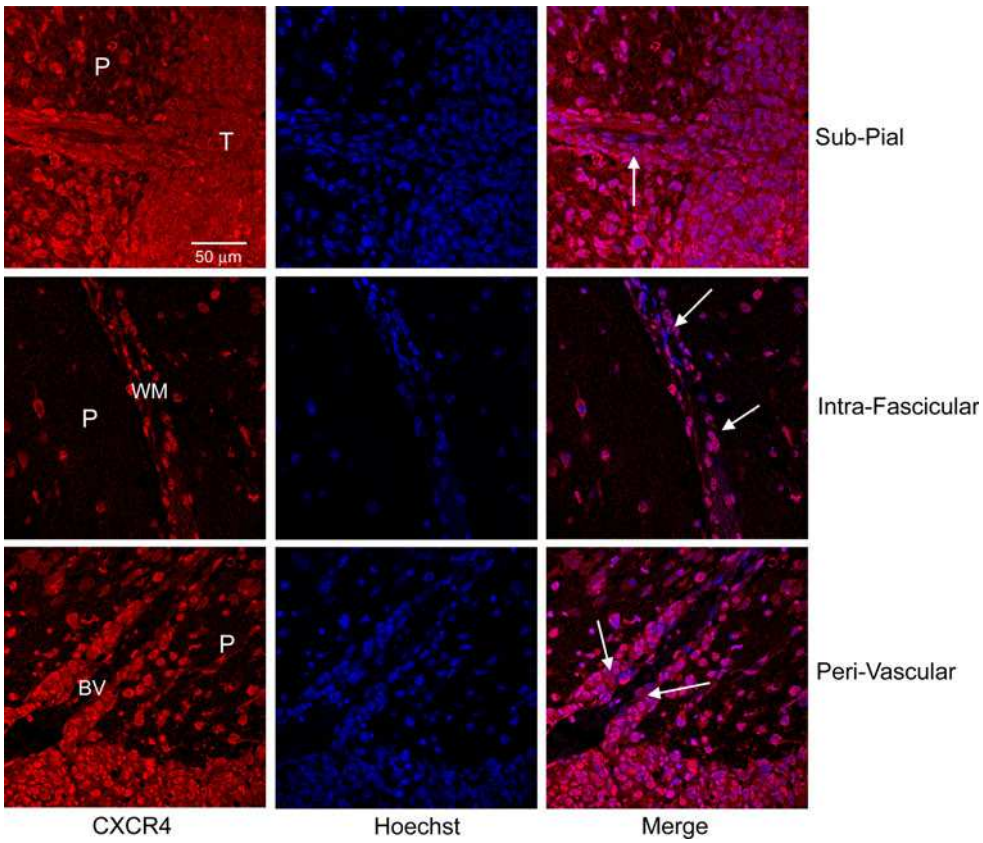

Fig. 8 Expression of CXCR4 in invasive VM-M3 tumor cells in vivo. CXCR4 protein localization was determined as described in "Methods" section. Images are shown at ×630. The *scale bar* is representative of all images shown. *Arrows* indicate regions of positive CXCR4 expression. The *arrow* in the *top panel* illustrates tumor cells invading into the brain parenchyma from the tumor mass (T) under the pial membrane. (*BV* blood vessel, *P* normal brain parenchyma, *T* tumor, *WM* white matter)

Ki-67 expression in VM-M3 tumors

As shown in Fig. 9, the VM-M3 tumors stain positive for the proliferation marker Ki-67, indicating a high proliferation rate of these cells in vivo. High Ki-67 expression was seen in tumor cells in the tumor core, as well as in invasive tumor cells found within the brain parenchyma. Invasive cells staining positive for Ki-67 include those cells migrating through the pial membrane (Fig. 9b), along blood vessels (Fig. 9b, arrow), through white matter tracts such as the corpus callosum (CC) (Fig. 9c, arrow) and into the brain parenchyma (Fig. 9d, arrow).

Discussion

Here we present a novel in vivo mouse model for brain tumor growth and invasion. Most available brain tumor models fall short of fully recapitulating all major characteristics of human GBM. An accurate in vivo model is necessary for the development of therapies that can target both local and distant tumor cell invasion. To date, no xenograft model or chemically induced rodent model displays the invasive characteristics of the VM-M3 model, to include sub-pial and ventricular spread, perivascular, perineuronal, peri- and intra-fascicular growth, and inter-hemispheric invasion. These routes of invasion have been referred to as the Secondary Structures of Scherer [4, 53]. These structures were identified in highly invasive human brain tumors to include GBM, astrocytoma, and oligodendroglioma [5, 53]. The secondary structures describe the growth of invasive tumor cells along the pre-existing structures of the nervous system and are independent of histological grade or cellular classification [5, 53]. This is important, as histological classification of brain tumor invasiveness can be ambiguous [54].

Although the murine GL261 glioma model also displays several invasive qualities of the VM-M3 brain tumor model, it does not express ventricular and inter-hemispheric spread and the invasive phenotype is limited to the invading edge of the tumor [19]. Additional advantages of the VM-M3 model include rapid and consistent growth patterns both in vivo and in vitro, a syngeneic host, and low immunogenicity as illustrated by robust growth at subcutaneous implantation sites [33, 40]. In vitro, the cells express two primary morphologies, which are cell cycle dependent. During division, the cells are small and round, but become flat and pancake shaped during the resting state as we previously described [33]. Though the VM-M3 cells predominately display the small and round morphology in vivo, additional pleomorphic cells are found throughout the tumor consistent with the cellular morphologies seen

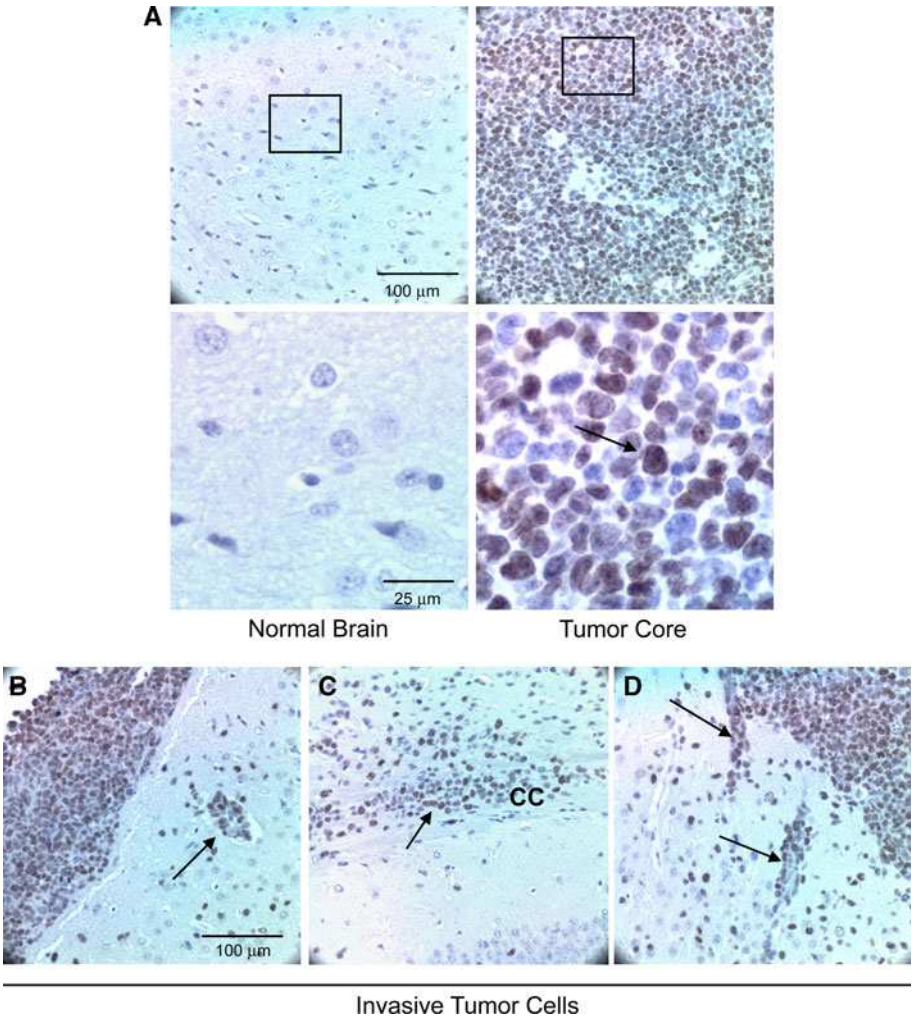

Fig. 9 Ki-67 expression in VM-M3 tumor. **a** Ki-67 expression in normal brain and in the tumor core was determined as described in "Methods" section. The *black boxes* from the *top panel* images are shown under higher digital zoom in the *bottom panel*. Ki-67 expression in the invasive tumor cells found migrating through the plal membrane (**b**), around blood vessels (**b**, *arrow*), within white matter (**c**), and invading into the brain parenchyma (**d**). Images are shown at ×400. *Scale bars* are representative of all images of that panel. *Arrows* indicate tumor cells staining positive for Ki-67 (*brown*). (*CC* corpus callosum)

human GBM [4]. VM-M3 cell growth and morphology is also consistent over multiple passages both in vivo and in vitro. The VM-M3 model is therefore unique in its ability to fully replicate the growth and invasive patterns of human GBM.

In addition to the similarities in growth, cell morphology, and invasion, the VM-M3 tumor also had genetic similarities with human GBM. Along with CXCR4 and Ki-67, a number of genetic markers have been linked to the invasive and aggressive phenotype of human GBM [55, 56]. Interestingly, insulin-like growth factor binding protein 2 (IGFBP-2) is known to be upregulated in human GBM [57, 58]. However, a more specific analysis revealed that IGFPB-2 is highly expressed in the cells of the tumor core, but is significantly down regulated in the cells along the invasive edge, suggesting that there is a distinct molecular signature in the invasive versus non-invasive cells within the same tumor [55]. We showed that the IGFBP-2 gene was highly expressed in the cells of the VM-NM1 tumor, which grows more rapidly but is less invasive than the VM-M3 tumor [33]. Our findings are consistent with those of a previous study showing IGFBP-2 expression in the core tumor cells of a GBM [55]. However, expression of IGFBP-2 was low in the VM-M3 invasive tumor cells, consistent with the expression profile of the invasive rim of human GBM [55].

The VM-M3 tumor is labeled with the firefly luciferase gene allowing for non-invasive detection of tumor growth and invasion via bioluminescent imaging. Bioluminescent imaging has been established as an accurate tool for measuring tumor growth over time [13, 46, 47]. As the VM-M3 tumor cells are invasive to all brain regions, we developed a novel bioluminescent-based quantitative assay for evaluating the extent of tumor invasion into the cortex, hippocampus, brain stem, and cerebellum. We showed that bioluminescence could be correlated with histological data on tumor growth and invasion. In contrast to histology, bioluminescent imaging is a more accurate measure of distal tumor cell invasion to multiple brain regions. This feature will allow for the quantitative assessment of potential therapies that target brain tumor invasion.

In conclusion we describe a novel model for malignant brain tumor growth and invasion. This model displays both genetic and behavioral characteristics of highly invasive human GBM. In addition, the tumor cells are labeled with the firefly luciferase gene allowing for non-invasive detection and quantitation of tumor growth. This model should be useful in assessing potential anti-invasive brain tumor therapies.

Acknowledgements This work was supported from NIH Grants [NS-055195; CA-102135] and from the Boston College Research expense fund. The authors would like to thank Roderick Bronson for technical advice and evaluation of tumor histology.

References

1. Wen PY, Kesari S (2008) Malignant gliomas in adults. N Engl J Med 359:492–507
2. Chang SM, Parney IF, Huang W, Anderson FA Jr, Asher AL, Bernstein M, Lillehei KO, Brem H, Berger MS, Laws ER (2005) Patterns of care for adults with newly diagnosed malignant glioma. JAMA 293:557–564
3. Laws ER Jr, Goldberg WJ, Bernstein JJ (1993) Migration of human malignant astrocytoma cells in the mammalian brain: Scherer revisited. Int J Dev Neurosci 11:691–697
4. Rubinstein LJ (1972) Tumors of the central nervous system. Armed Forces Institute of Pathology, Washington, DC
5. Scherer HJ (1940) The forms of growth in gliomas and their practical significance. Brain 63:1–34
6. Duffner PK (2006) The long term effects of chemotherapy on the central nervous system. J Biol 5:21
7. Szatmari T, Lumniczky K, Desaknai S, Trajcevski S, Hidvegi EJ, Hamada H, Safrany G (2006) Detailed characterization of the mouse glioma 261 tumor model for experimental glioblastoma therapy. Cancer Sci 97:546–553
8. Huse JT, Holland EC (2009) Genetically engineered mouse models of brain cancer and the promise of preclinical testing. Brain Pathol (Zurich, Switzerland) 19:132–143
9. Candolfi M, Curtin JF, Nichols WS, Muhammad AG, King GD, Pluhar GE, McNiel EA, Ohlfest JR, Freese AB, Moore PF, Lerner J, Lowenstein PR, Castro MG (2007) Intracranial glioblastoma models in preclinical neuro-oncology: neuropathological characterization and tumor progression. J Neurooncol 85:133–148
10. Xie Q, Thompson R, Hardy K, DeCamp L, Berghuis B, Sigler R, Knudsen B, Cottingham S, Zhao P, Dykema K, Cao B, Resau J, Hay R, Vande Woude GF (2008) A highly invasive human glioblastoma pre-clinical model for testing therapeutics. J Transl Med 6:77
11. Fomchenko EI, Holland EC (2006) Mouse models of brain tumors and their applications in preclinical trials. Clin Cancer Res 12:5288–5297
12. Martinez-Murillo R, Martinez A (2007) Standardization of an orthotopic mouse brain tumor model following transplantation of CT-2A astrocytoma cells. Histol Histopathol 22:1309–1326
13. Maes W, Deroose C, Reumers V, Krylyshkina O, Gijsbers R, Baekelandt V, Ceuppens J, Debyser Z, Van Gool SW (2008) In vivo bioluminescence imaging in an experimental mouse model for dendritic cell based immunotherapy against malignant glioma. J Neurooncol 91(2):127-139
14. Mukherjee P, El-Abbadi MM, Kasperzyk JL, Ranes MK, Seyfried TN (2002) Dietary restriction reduces angiogenesis and growth in an orthotopic mouse brain tumour model. Br J Cancer 86:1615–1621
15. Mukherjee P, Abate LE, Seyfried TN (2004) Antiangiogenic and proapoptotic effects of dietary restriction on experimental mouse and human brain tumors. Clin Cancer Res 10:5622–5629
16. Barth RF (1998) Rat brain tumor models in experimental neuro-oncology: the 9L, C6, T9, F98, RG2 (D74), RT-2 and CNS-1 gliomas. J Neurooncol 36:91–102
17. Vince GH, Bendszus M, Schweitzer T, Goldbrunner RH, Hildebrandt S, Tilgner J, Klein R, Solymosi L, Christian Tonn J, Roosen K (2004) Spontaneous regression of experimental gliomas—an immunohistochemical and MRI study of the C6 glioma spheroid implantation model. Exp Neurol 190:478–485
18. Kruse CA, Molleston MC, Parks EP, Schiltz PM, Kleinschmidt-DeMasters BK, Hickey WF (1994) A rat glioma model, CNS-1, with invasive characteristics similar to those of human gliomas: a comparison to 9L gliosarcoma. J Neurooncol 22:191–200
19. Zagzag D, Esencay M, Mendez O, Yee H, Smirnova I, Huang Y, Chiriboga L, Lukyanov E, Liu M, Newcomb EW (2008) Hypoxia- and vascular endothelial growth factor-induced stromal cell-derived factor-1alpha/CXCR4 expression in glioblastomas: one plausible explanation of Scherer's structures. Am J Pathol 173:545–560
20. Holland EC (2001) Gliomagenesis: genetic alterations and mouse models. Nat Rev Genet 2:120–129
21. Hu X, Holland EC (2005) Applications of mouse glioma models in preclinical trials. Mutat Res 576:54–65
22. Dai C, Holland EC (2001) Glioma models. Biochim Biophys Acta 1551:M19–M27
23. Louis DN (2006) Molecular pathology of malignant gliomas. Annu Rev Pathol 1:97–117
24. Parsons DW, Jones S, Zhang X, Lin JC, Leary RJ, Angenendt P, Mankoo P, Carter H, Siu IM, Gallia GL, Olivi A, McLendon R, Rasheed BA, Keir S, Nikolskaya T, Nikolsky Y, Busam DA, Tekleab H, Diaz LA Jr, Hartigan J, Smith DR, Strausberg RL, Marie SK, Shinjo SM, Yan H, Riggins GJ, Bigner DD, Karchin R, Papadopoulos N, Parmigiani G, Vogelstein B, Velculescu VE, Kinzler KW (2008) An integrated genomic analysis of human glioblastoma multiforme. Science (New York, NY) 321:1807–1812
25. Assanah M, Lochhead R, Ogden A, Bruce J, Goldman J, Canoll P (2006) Glial progenitors in adult white matter are driven to form malignant gliomas by platelet-derived growth factor-expressing retroviruses. J Neurosci 26:6781–6790
26. Heidner GL, Kornegay JN, Page RL, Dodge RK, Thrall DE (1991) Analysis of survival in a retrospective study of 86 dogs with brain tumors. J Vet Intern Med 5:219–226
27. LeCouteur RA (1999) Current concepts in the diagnosis and treatment of brain tumours in dogs and cats. J Small Anim Pract 40:411–416
28. Lipsitz D, Higgins RJ, Kortz GD, Dickinson PJ, Bollen AW, Naydan DK, LeCouteur RA (2003) Glioblastoma multiforme: clinical findings, magnetic resonance imaging, and pathology in five dogs. Vet Pathol 40:659–669
29. Foster ES, Carrillo JM, Patnaik AK (1988) Clinical signs of tumors affecting the rostral cerebrum in 43 dogs. J Vet Intern Med 2:71–74
30. Fraser H (1971) Astrocytomas in an inbred mouse strain. J Pathol 103:266–270
31. Fraser H (1986) Brain tumours in mice, with particular reference to astrocytoma. Food Chem Toxicol 24:105–111
32. Morantz RA, Wood GW, Foster M, Clark M, Gollahon K (1979) Macrophages in experimental and human brain tumors. Part 2: studies of the macrophage content of human brain tumors. J Neurosurg 50:305–311

33. Huysentruyt LC, Mukherjee P, Banerjee D, Shelton LM, Seyfried TN (2008) Metastatic cancer cells with macrophage properties: evidence from a new murine tumor model. Int J Cancer 123:73–84
34. Rossi ML, Jones NR, Candy E, Nicoll JA, Compton JS, Hughes JT, Esiri MM, Moss TH, Cruz-Sanchez FF, Coakham HB (1989) The mononuclear cell infiltrate compared with survival in high-grade astrocytomas. Acta Neuropathol Berl 78:189–193
35. Roggendorf W, Strupp S, Paulus W (1996) Distribution and characterization of microglia/macrophages in human brain tumors. Acta Neuropathol 92:288–293
36. Stevenson CB, Ehtesham M, McMillan KM, Valadez JG, Edgeworth ML, Price RR, Abel TW, Mapara KY, Thompson RC (2008) CXCR4 expression is elevated in glioblastoma multiforme and correlates with an increase in intensity and extent of peritumoral T2-weighted magnetic resonance imaging signal abnormalities. Neurosurgery 63:560–569 (discussion 569–570, 2008)
37. Bian XW, Yang SX, Chen JH, Ping YF, Zhou XD, Wang QL, Jiang XF, Gong W, Xiao HL, Du LL, Chen ZQ, Zhao W, Shi JQ, Wang JM (2007) Preferential expression of chemokine receptor CXCR4 by highly malignant human gliomas and its association with poor patient survival. Neurosurgery 61:570–578 (discussion 578–579, 2007)
38. Ehtesham M, Stevenson CB, Thompson RC (2008) Preferential expression of chemokine receptor CXCR4 by highly malignant human gliomas and its association with poor patient survival. Neurosurgery 63:E820 (author reply E820)
39. El-Abbadi M, Seyfried TN, Yates AJ, Orosz C, Lee MC (2001) Ganglioside composition and histology of a spontaneous metastatic brain tumour in the VM mouse. Br J Cancer 85:285–292
40. Huysentruyt LC, Shelton LM, Seyfried TN (2010) Influence of methotrexate and cisplatin on tumor progression and survival in the VM mouse model of systemic metastatic cancer. Int J Cancer 126(1):65–72
41. Ng WH, Yeo TT, Kaye AH (2005) Spinal and extracranial metastatic dissemination of malignant glioma. J Clin Neurosci 12:379–382
42. Hoffman HJ, Duffner PK (1985) Extraneural metastases of central nervous system tumors. Cancer 56:1778–1782
43. Kauffman HM, Cherikh WS, McBride MA, Cheng Y, Hanto DW (2007) Deceased donors with a past history of malignancy: an organ procurement and transplantation network/united network for organ sharing update. Transplantation 84:272–274
44. Lopes MBS, Vanbenberg SR, Scheithauer BW (1993) The world health organization classification of nervous system tumors in experimental neuro-oncology. In: Schmidek HH, Levine AJ (eds) Molecular genetics of nervous system tumors. Wiley, New York, pp 1–36
45. Liwnicz BH, Rubinstein LJ (1979) The pathways of extraneural spread in metastasizing gliomas: a report of three cases and critical review of the literature. Hum Pathol 10:453–467
46. Deroose CM, Reumers V, Gijsbers R, Bormans G, Debyser Z, Mortelmans L, Baekelandt V (2006) Noninvasive monitoring of long-term lentiviral vector-mediated gene expression in rodent brain with bioluminescence imaging. Mol Ther 14:423–431
47. Szentirmai O, Baker CH, Lin N, Szucs S, Takahashi M, Kiryu S, Kung AL, Mulligan RC, Carter BS (2006) Noninvasive bioluminescence imaging of luciferase expressing intracranial U87 xenografts: correlation with magnetic resonance imaging determined tumor volume and longitudinal use in assessing tumor growth and antiangiogenic treatment effect. Neurosurgery 58:365–372 (discussion 365–372, 2006)
48. Ranes MK, El-Abbadi M, Manfredi MG, Mukherjee P, Platt FM, Seyfried TN (2001) N-butyldeoxynojirimycin reduces growth and ganglioside content of experimental mouse brain tumours. Br J Cancer 84:1107–1114
49. Seyfried TN, el-Abbadi M, Roy ML (1992) Ganglioside distribution in murine neural tumors. Mol Chem Neuropathol 17:147–167
50. Shapiro WR, Ausman JI, Rall DP (1970) Studies on the chemotherapy of experimental brain tumors: evaluation of 1,3-bis(2-chloroethyl)-l-nitrosourea, cyclophosphamide, mithramycin, and methotrexate. Cancer Res 30:2401–2413
51. Huysentruyt LC, Mukherjee P, Banerjee D, Shelton LM (2008) Metastatic cancer cells with macrophage properties: Evidence from a new murine tumor model. J Natl Cancer Inst 46(2):359–368
52. Abate LE, Mukherjee P, Seyfried TN (2006) Gene-linked shift in ganglioside distribution influences growth and vascularity in a mouse astrocytoma. J Neurochem 98:1973–1984
53. Scherer HJ (1938) Structural development in gliomas. Am J Cancer 34:333–351
54. Scherer HJ (1940) The pathology of cerebral gliomas. A critical review. J Neurol 34:147–177
55. Hoelzinger DB, Mariani L, Weis J, Woyke T, Berens TJ, McDonough WS, Sloan A, Coons SW, Berens ME (2005) Gene expression profile of glioblastoma multiforme invasive phenotype points to new therapeutic targets. Neoplasia (New York, NY) 7:7–16
56. Li SW, Qiu XG, Chen BS, Zhang W, Ren H, Wang ZC, Jiang T (2009) Prognostic factors influencing clinical outcomes of glioblastoma multiforme. Chin Med J 122:1245–1249
57. Rickman DS, Bobek MP, Misek DE, Kuick R, Blaivas M, Kurnit DM, Taylor J, Hanash SM (2001) Distinctive molecular profiles of high-grade and low-grade gliomas based on oligonucleotide microarray analysis. Cancer Res 61:6885–6891
58. Fuller GN, Rhee CH, Hess KR, Caskey LS, Wang R, Bruner JM, Yung WK, Zhang W (1999) Reactivation of insulin-like growth factor binding protein 2 expression in glioblastoma multiforme: a revelation by parallel gene expression profiling. Cancer Res 59:4228–4232